Atmos. Chem. Phys. Discuss., 12, 25573–25615, 2012
www.atmos-chem-phys-discuss.net/12/25573/2012/
doi:10.5194/acpd-12-25573-2012

Atmospheric Chemistry and Physics Discussions

CLARA-SAL: a global 28-yr timeseries of Earth's black-sky surface albedo

A. Riihelä[1], **T. Manninen**[1], **V. Laine**[1], **K. Andersson**[2], **and F. Kaspar**[3]

[1]Finnish Meteorological Institute, P.O. Box 503, 00101 Helsinki, Finland
[2]VTT Technical Research Center of Finland, Espoo, Finland
[3]Deutscher Wetterdienst, Offenbach, Germany

Received: 10 July 2012 – Accepted: 13 September 2012 – Published: 26 September 2012

Correspondence to: A. Riihelä (aku.riihela@fmi.fi)

Published by Copernicus Publications on behalf of the European Geosciences Union.

Abstract

We present a novel 28-yr dataset of Earth's black-sky surface albedo, derived from AVHRR instruments. The dataset is created using algorithms to separately derive the surface albedo for different land use areas globally. Snow, sea ice, open water and vegetation are all treated independently. The product features corrections for the atmospheric effect in satellite-observed surface radiances, a BRDF correction for the anisotropic reflectance properties of natural surfaces, and a novel topography correction of geolocation and radiometric accuracy of surface reflectance observations over mountainous areas. The dataset is based on a homogenized AVHRR radiance timeseries. The product is validated against quality-controlled in situ observations of clear-sky surface albedo at various BSRN sites around the world. Snow and ice albedo retrieval validation is given particular attention using BSRN sites over Antarctica, Greenland Climate Network stations on the Greenland Ice Sheet (GrIS), as well as sea ice albedo data from the SHEBA and Tara expeditions. The product quality is found to be comparable to other previous long-term surface albedo datasets from AVHRR.

1 Introduction

Accurate determination of Earth's surface albedo is required for both characterizing the atmosphere-surface boundary layer in atmospheric studies, and resolving the radiative budget at surface level for climate monitoring studies. Most such studies require the surface albedo to be known over a large area with continuous monitoring. Global climate studies naturally require global coverage, which is difficult to attain using airborne or in situ observation methods. Satellite-based surface albedo estimation methods provide both continuous monitoring and fully global coverage from polar orbits.

A limiting factor from the viewpoint of climate studies is the temporal coverage of satellite data. Homogeneous surface albedo datasets often cover only the lifespan of one or two satellites, while climate studies would benefit more from data records of

ACPD
12, 25573–25615, 2012

longer length (Trenberth et al., 2006). The Advanced Very High Resolution Radiometer (AVHRR) instrument has flown on all polar-orbiting National Oceanic and Atmospheric Administration (NOAA) weather satellites, providing the longest continuous timeseries of observations on the reflectance properties of Earth. Once intercalibrated, this timeseries provides a basis for generating a long-term global dataset on surface albedo.

In this paper, we introduce and validate a new 28-yr timeseries (1982–2009) of Earth's surface albedo, derived from AVHRR/2 and AVHRR/3 sensors. The timeseries has been created in the Satellite Application Facility on Climate Monitoring (CM SAF) project of EUMETSAT as a part of the CMSAF cLouds, Albedo and RAdiation (CLARA) product family (Karlsson et al., 2012). This timeseries, henceforth called CLARA-SAL (from Surface ALbedo), describes the global broadband (0.25–2.5 µm) Directional-Hemispherical Reflectance (DHR) of terrestrial surfaces – or black-sky albedo as it is also known. In addition to describing the dataset characteristics and the processing algorithm behind it, we will also present results from an extensive validation effort aimed at determining the albedo retrieval accuracy. This paper specifically describes the first edition of the CLARA-SAL dataset, formally belonging to the CLARA-A1 dataset family (A for AVHRR, 1 for first edition).

This paper is organized as follows. We will first provide a review of current surface albedo datasets covering at least several years and briefly discuss their major characteristics. Then we proceed to an overview of the CLARA-SAL product and its main properties including spatial and temporal coverage. The discussion then goes deeper into the SAL algorithm itself as we describe the process of retrieving surface albedo from the AVHRR measurements. The algorithm description is followed by an overview of the validation results to date and a discussion on the main findings, including the perceived strengths and weaknesses of the dataset. For reference, we also provide a comparison of CLARA-SAL to the often-used Moderate Resolution Imaging Spectroradiometer (MODIS) MCD43C3 albedo products. We finish with a brief outlook on future development directions for next editions of the CLARA-SAL dataset, and conclusions.

ACPD
12, 25573–25615, 2012

2 Satellite-derived surface albedo timeseries

2.1 On surface albedo terminology

The surface albedo of natural surfaces is determined by the inherent optical properties of the surface material, as well as the properties of the atmosphere affecting the incoming and reflected radiation fluxes. Therefore the definition of surface albedo changes depending on whether or not atmospheric effects are included. In the literature, the surface albedo where the incoming radiation flux is unidirectional without any atmospheric effects is called the Directional-Hemispherical Reflectance (DHR), often also called "black-sky albedo". If the incoming radiation flux is completely diffuse, the surface albedo is defined as the Bi-Hemispherical Reflectance (BHR), or "white-sky albedo". Under natural illumination conditions, the incoming radiation flux at Earth surface is a varying combination of direct and diffuse radiation fluxes. Therefore, the observable albedo at Earth surface level is also a weighted combination of DHR and BHR according to cloudiness, atmospheric characteristics, and Sun Zenith Angle (SZA). This albedo is often called "blue-sky albedo". For the remainder of this paper, we shall use this terminology to describe the various albedo quantities in accordance with, e.g. Schaepman-Strub et al. (2006) and Lucht et al. (2000).

2.2 Previous long-term surface albedo timeseries

Several research teams have produced long-term timeseries of surface albedo from various satellite instruments. Here we will briefly review the datasets that are 10+ years in length. Wang and Key (2005) described the AVHRR Polar Pathfinder dataset, which contains broadband directional-hemispheric apparent (blue-sky) surface albedo from the polar regions between 1982–1999. This dataset has since been extended to cover 1982–2004 in the APP-x version.

Lucht et al. (2000) introduced the MODIS surface albedo algorithm, which has since been applied to MODIS data from the Terra and Aqua satellites to produce a global

ACPD
12, 25573–25615, 2012

surface albedo timeseries from the year 2000 to the present day. The MODIS dataset provides both black-sky and white-sky albedo. Flying on the same satellite platforms and utilizing MODIS data as background information, the CERES instrument has been used to derive global broadband black-sky albedo from the year 2000 onwards (Rutan et al., 2009).

Loew and Govaerts (2010) describe a surface albedo timeseries spanning 1982–2006 generated from the geostationary Meteosat First Generation (MFG) imager data. There are also current efforts underway to extend the algorithm to other geostationary weather satellite data (Govaerts et al., 2008).

The NASA/GEWEX surface radiation budget project has produced surface radiative fluxes spanning 1983–2007 by utilizing a combination of ISCCP DX satellite radiances (Rossow and Schiffer, 1999) and various reanalysis datasets. More details may be found in Stackhouse et al. (2011). The ISCCP project has also produced their own radiative fluxes for the same period (Zhang et al., 2004).

3 The characteristics of the CLARA-SAL dataset

3.1 Dataset coverage

The dataset coverage is global over a pentad (five days) or one month period. The provided CLARA-SAL surface albedo is the average of all Global Area Coverage (GAC)-resolution albedo retrievals per grid point per time period. Swath-level processing takes place at the nominal GAC resolution (4.4 km at nadir), but the spatial resolution in the global temporal mean products is 0.25° on a regular latitude-longitude grid. We have also reprojected the GAC-resolution albedo retrievals over the polar regions to an equal-area projection (EASE-grid) with a grid size of 25 km. Two examples of the monthly mean products are shown in Figs. 1 (Arctic) and 2 (global).

Along with the temporal mean albedo, each product also contains the number of observations from which the mean is calculated (per grid cell), and the standard deviation

ACPD
12, 25573–25615, 2012

of the retrievals in each grid cell. We recommend that users consider and utilize these data as a quality assurance measure when using the CLARA-SAL products. We have also calculated histograms of the albedo retrievals over the globe with a 0.02 bin size. These histograms are available to users upon request. All products are provided free of charge to any interested users.

3.2 The CLARA-SAL retrieval algorithm

The CLARA-SAL algorithm follows a sequential approach, first correcting the TOA reflectances from AVHRR channels 1 and 2 for topography and atmospheric effects for all pixels, and then utilizing different algorithms according to each pixel's land cover to convert the spectral surface reflectances into a broadband surface albedo. Snow surfaces are an exception, as the image swath processing is intended to only yield bidirectional broadband snow reflectances. During postprocessing, the retrieved bidirectional snow reflectances over the viewing hemisphere are spatiotemporally averaged to produce a black-sky snow broadband albedo value at each end product grid cell.

The CLARA-SAL albedo retrieval is based on a homogenized TOA radiance data record across the entire AVHRR instrument family timeline. The radiance data record is constructed using the method described by Heidinger et al. (2010). This homogenization of the underlying radiance data record significantly diminishes albedo variation resulting from differences in calibration across the 11 different AVHRR instruments. This radiance data record is common to all CLARA products (Karlsson et al., 2012).

Here we briefly list the main stages of CLARA-SAL retrievals. More details on the process may be found in Appendix A, and the CLARA-SAL Algorithm Theoretical Basis Document (ATBD). After the initial topography correction for geolocation and radiometry, the atmospheric effects are corrected for using the Simplified Method for Atmospheric Correction (SMAC) after Rahman and Dedieu (1994). AOD and O_3 content of the atmosphere are kept constant at 0.1 and 0.35 (atm cm), respectively. The subsequent effect on retrievals is analyzed in Sect. 7. Then, anisotropic reflectance (over vegetated/barren surfaces) is corrected and the surface reflectances are converted into

ACPD
12, 25573–25615, 2012

spectral albedo after Wu et al. (1995) and Roujean et al. (1992). Broadband albedo is retrieved according to land cover type. Over vegetation, the spectral albedos are processed using a narrow-to-broadband conversion algorithm by Liang (2000). Water surface albedo is presently derived from a LUT by Jin et al. (2004). As wind speed or chlorophyll data was not included in this first version, the water surface albedo is in fact a constant 0.0676. For snow surfaces, the broadband conversion is performed after Xiong et al. (2002).

4 Validation of the dataset against in situ albedo observations

4.1 Validation methods

The validation of this first release of the CLARA-SAL dataset was done using in situ albedo observations from the SHEBA and Tara ice camps and Baseline Surface Radiation Network (BSRN) and Greenland Climate Network (GC-Net) station networks as reference data (Ohmura et al., 1998; Steffen et al., 1996). Eight BSRN stations and three GC-Net stations were used as validation sites. The main criteria for selection of the sites was sufficient temporal coverage. Apart from the ice camp sites, we required more than 10 yr of in situ data to be available to include the site in the validation. The sites are listed in Table 1 and their locations are shown in Fig. 2. The in situ albedo data covers vegetated terrain, coastal sites, seasonal and perennial snow cover, and sea ice.

For the validation to be accurate, the satellite and in situ data should have similar spectral coverage, be temporally and spatially colocated, and the in situ observations should be spatially representative for the satellite footprint area. We address each of these requirements in turn.

The albedo measurements at the BSRN sites and Sodankylä are performed using broadband albedometers (typical coverage 0.285–2.8 µm), therefore we do not need to adjust their data to achieve a spectral match with CLARA-SAL. The GC-Net

ACPD
12, 25573–25615, 2012

observations are taken using LI-COR 200 SZ pyranometers that observe a narrower band (0.4–1.1 µm). (Stroeve et al., 2001) reported differences of up to 4 % relative to concurrently measured broadband albedo to result from the narrower observation band in these sensors. We include this additional uncertainty in the GC-Net in situ data in the validation accuracy considerations.

We need to also consider the atmospheric effects in the in situ measurements. Albedo sensors (pyranometer pairs) measure incoming and reflected radiation fluxes simultaneously to determine the surface albedo (the so-called blue sky albedo). The incoming radiation flux in real world conditions consists of both direct and diffuse radiation fluxes. To match this data perfectly to the CLARA-SAL black-sky albedo, we would need to remove all diffuse flux contributions (resulting from atmospheric scattering), and also account for any possible absorption effects in the direct flux. However, Liu et al. (2009) showed in their study that the difference between black-sky and blue-sky albedo is very small in cloudfree conditions when SZA is less than 70°. Manninen et al. (2012) showed that the difference between black-sky and blue-sky albedo measurements on the ground at Cabauw in the Netherlands is typically no more than 5 %, although the difference increases with increasing AOD. Considering these results, we choose not to adjust the in situ measurements for any blue-sky/black-sky albedo difference. This decision is also supported by the fact that our validation strategy is based on exclusive selection of confirmed clear-sky in situ data for validation reference, based on the CM SAF cloud mask product Karlsson et al. (2012). Sites where typical AOD concentrations are large will most likely show poorer correspondence in any case owing to the constant AOD in the atmospheric correction.

As stated, temporal colocation is achieved by storing the date-time stamps of cloud-free AVHRR overpasses at our validation sites and then exclusively selecting corresponding in situ observations to form the reference albedo for the pentad or month in question. Spatial colocation and representativeness of the in situ measurement for the GAC footprint are more challenging issues. We will next discuss a method to

ACPD
12, 25573–25615, 2012

quantitatively assess the site representativeness for validating satellite-based albedo measurements.

4.2 Using semivariogram estimators to assess site representativeness

In geostatistics, semivariograms are used to describe the spatial autocorrelation of measurements. Semivariograms illustrate the similarity of measurements at increasing distance (lag) relative to a reference point and therefore quantify the representativeness of a single site for a larger area. Calculation of an empirical semivariogram from measurement data requires that the data is continuous, which is generally true for optical satellite observations of snow-free (or completetely snow-covered) Earth's surface. The empirical semivariogram (also called semivariogram estimator) may be calculated as (Matheron, 1963)

$$\hat{\gamma}(h) = \frac{1}{2N(h)} \sum_{i=1}^{N(h)} [z(x_i + h) - z(x_i)]^2 \quad (1)$$

where $N(h)$ is the number of data pairs $(z(x_i + h), z(x_i))$ at distance h from each other.

Recently Susaki et al. (2007) and Román et al. (2009) have applied semivariogram analysis into assessing site representativeness in MODIS albedo product validation over rice paddies and forests. Their work was based on calculating albedo estimates from 30-m resolution Landsat ETM+ images and then applying theoretical semivariogram models to analyze their variability within MODIS spatial resolution scales. We follow the general approach of their studies, but provide a simpler method of quantifying the site representativeness.

We use Landsat TM/ETM+ near-infrared (band 4) surface reflectance images at our validation sites over summer to analyze site representativeness. We calculate the empirical omnidirectional semivariogram at each site up to a maximum lag distance of half of the CLARA-SAL 0.25° pixel diagonal, using lag distance multiples of 30 m (TM/ETM+ resolution). Rather than fitting a semivariogram model to this empirical data,

ACPD
12, 25573–25615, 2012

we then calculate its area integral and compare it to the mean CLARA-SAL RMSE at the site over the summer months. In essence, we replace the physical interpretation of a theoretical semivariogram model (range and sill) with an empirical measure of the cumulative variability of near-infrared surface reflectance with respect to the site location.

We choose to use near-infrared surface reflectance in lieu of calculating surface albedo estimates to simplify the calculations by removing the need for a BRDF correction and a narrow-to-broadband conversion. Also, the near-infrared surface reflectance tends to dominate the broadband AVHRR surface albedo based on wide visible and NIR spectral bands (Liang, 2000). Therefore application of NIR surface reflectances as a proxy to actual surface albedo data is acceptable for vegetated sites over snow-free periods. As stated by Román et al. (2009), accurate determination of satellite field-of-view on the ground is challenging. In AVHRR-LAC data, geolocation uncertainty can be half a pixel or more (Lucht et al., 2000). We therefore simplify the analysis by calculating the semivariograms centered on the validation site. We also calculate the semivariogram omnidirectionally to better observe the overall variability of surface reflectance in the region surrounding the site.

4.3 Validation results over land and snow

To maintain clarity and brevity, we do not show full validation result details here for all 10 sites. We highlight BSRN sites in the US (Southern Great Plains) and Central Europe (Payerne), and one GC-Net site with perennial snow cover (Summit camp, Greenland) for a detailed analysis.

4.3.1 Southern Great Plains BSRN site

The Southern Great Plains (SGP) site, located in Central Oklahoma and operated by the Atmospheric Radiation Measurement (ARM) program of the US government, offers the longest continuous in situ measurement timeseries in our study. The site is located

ACPD
12, 25573–25615, 2012

in a rural area with negligible topography. Aside from sporadic snowfall events in the December / January timeframe, the albedo of the site is quite stable around 0.2.

We show the relative retrieval error of CLARA-SAL products between 1994–2009 at SGP in Fig. 3. The variability of retrieval error is larger in the early part of the timeseries when satellite data is more sparse, and pentad means in general are more vulnerable to errors induced by partial snow cover affecting either in situ observation but not the satellite product (or vice versa), as well as cloud masking errors.

We display the overall achieved retrieval accuracy as RMSE units and mean relative retrieval errors over year-quarters in Table 2. Both pentad and monthly mean RMSEs are low (≈ 0.04), and the relative retrieval errors are on the order of $-10\,\%$ regardless of season. The seasonally invariant retrieval accuracy is a result of the (intra-annually) largely invariant in situ albedo of the site. The interannual variability of the in situ albedo at SGP is also small (not shown). The fairly homogeneous cropland surrounding the site suggests good spatial representativeness of the in situ albedo over the satellite footprint; we will return to the topic in detail in Sect. 6.

4.3.2 Payerne BSRN site

The Payerne BSRN site is located in Western Switzerland and is operated by MeteoSwiss. The site is located at the border of the town of Payerne, outside the town agricultural land cover dominates. The pyranometers used in this study are located 2 m above a grass field.

Like SGP, Payerne also experiences occasional snowfall during the winter period. A notable difference to SGP is that the grid-averaged CLARA-SAL products are substantially negatively biased. As the validation results in Table 2 show, RMSE of both pentad and monthly means is considerably larger here than at SGP, and relative retrieval errors of $-40\,\%$ or more are common. However, we have analysed the instantaneous albedo retrievals at the higher GAC resolution and found a considerably smaller bias (RMSE 0.055). This points towards spatial representativeness issues at this validation site.

ACPD
12, 25573–25615, 2012

The overall retrieval accuracy during the validation period is illustrated in Fig. 4 and expressed numerically in Table 2. We will show in Sect. 4.5 that problems in site representativeness are a likely cause of the observed negative bias.

4.3.3 Summit camp, Greenland

The Greenland Environmental Observatory, informally Summit camp, is situated near the highest point of the Greenland Ice Sheet. The ice sheet under the camp is over 3000 m thick. The altitude combined with the large distance from coast create conditions in which the perennial on-site snow cover does not melt even during midsummer. The albedo over the central part of the ice sheet is therefore very stable. This site has been used extensively in past MODIS snow albedo retrieval validation by Stroeve et al. (2005, 2006).

The full validation period retrieval accuracy is illustrated in Fig. 5 and listed in Table 2.

The results show a good and stable retrieval accuracy over the entire period. The results are similar to the initial validation results for this retrieval method shown by Riihelä et al. (2010). It should be noted that the instantaneous CLARA-SAL retrievals are bidirectional broadband surface reflectance estimates, therefore still containing reflectance anisotropy effects. The pentad and monthly means provide a good estimate of the surface albedo, although minor overestimations occur during spring and summer.

We further note that the good retrieval accuracy is also a result of well-matched atmospheric parameters. The atmosphere over Greenland is typically dry and has few aerosols (Stroeve et al., 1997). Therefore the constant AOD of 0.1 used in this edition of CLARA-SAL data is an acceptable approximation of prevailing conditions. The outliers showing significant underestimates are nearly always a result of cloud mask misclassifications over a bright snow surface.

ACPD
12, 25573–25615, 2012

4.4 Validation results over sea ice

For assessing CLARA-SAL retrieval quality over sea ice, we utilize surface broadband albedo observations from the Tara (Gascard et al., 2008) and Surface Heat Budget of the Arctic Ocean (SHEBA) (Perovich et al., 2002) floating ice camps as reference data. The changing location of the ice camps is accounted for when selecting CLARA-SAL grid cells for validation. To better assess the capacity of CLARA-SAL in tracking the changing albedo of Arctic sea ice over polar summer, we focus our validation on pentad mean products.

4.4.1 SHEBA validation

Our validation study utilizes SHEBA surface broadband albedo data from May 1998 to September 1998 to match satellite data availability. The location of the ice camp was in the region between 76–80° N and 158–168° W. The SHEBA measurements were taken along a 200 m transect one to three times a week; we calculate the mean albedo of the transect to serve as the site albedo. SHEBA cloudiness observations (Intrieri et al., 2002) are studied to identify cloudy skies situations for exclusion. However, the data showed that the vast majority of measurement days had cloud cover on-site for large parts of the day. Culling the reference dataset to include only clear-sky data would therefore also render it too small to draw conclusions about the performance of the satellite retrieval. We thus choose to include all measured transects into the validation, noting that cloudiness typically increases the broadband albedo of sea ice by 5–10 %, depending on cloud thickness and the existence of snow cover and/or melt ponds on the ice (Key et al., 2001; Grenfell and Perovich, 1984).

Figure 6 shows the achieved retrieval accuracy at pentad mean level against SHEBA observations. CLARA-SAL clearly tracks the overall evolution of the sea ice pack from its dry snow phase through the snowmelt onset and melt pond formation phases. CLARA-SAL performance during late summer decreases as the Sun Zenith Angles

ACPD
12, 25573–25615, 2012

grow large, causing problems for both cloud identification and albedo estimation from fewer available data. Achieved RMSE for the pentad mean retrievals is 0.081.

4.4.2 Tara validation

The in situ albedo observations at Tara ice camp took place with a fixed instrument measuring continuously as the schooner Tara drifted with the sea ice across the Arctic Ocean. While Tara was icebound between September 2006 and January 2008, we focus our study on polar summer 2007 when SAL is available. We have utilized hourly all-sky albedo measurements to compose the in situ pentad mean albedo in order to maintain cohesion with the SHEBA validation. Figure 7 shows the retrieval accuracy of CLARA-SAL relative to the albedo observations at Tara ice camp. The RMSE of the retrieval over this dataset is 0.090, similar to the SHEBA results.

In a previous study, Riihelä et al. (2010) compared Tara albedo data to the higher-resolution operational SAL product of CM SAF. They found a better retrieval accuracy (RMSE of 0.045) when comparing only against confirmed clear-sky in situ data from Tara, although the exclusion also limited the data set significantly compared to this study. Since cloudy conditions were dominant during the Tara study period, we tested the effect of the estimated +0.05 difference between sea ice albedo under cloudy and clear sky. Assuming the Tara in situ data to correspond mainly to cloudy sky albedo, we subtracted 0.05 from each sample and recalculated the RMSE, improving it to 0.067. As the CLARA-SAL grid is coarser than that used by Riihelä et al. (2010), we can hypothesize that much of the remaining difference is due to increased heterogeneity of the satellite observations in the larger CLARA-SAL grid cell over Tara.

4.5 Site representativeness analysis

The validation results from land-based sites in Table 2 show considerable variability. To investigate how much of this variability may be explained by surface albedo heterogeneity within the CLARA-SAL grid cell, we performed a semivariogram analysis over

ACPD
12, 25573–25615, 2012

our five validation sites located over vegetated areas (Barrow, SGP, Tateno, Sodankylä, and Payerne). Payerne and SGP have already been discussed in detail. Barrow is located on the north coast of Alaska, the region has tundra vegetation and several small lakes and ponds. Sodankylä is in Northern Finland, the site is surrounded by boreal forest stands and mires. Tateno site is located north of Tokyo, the site is surrounded by suburban and urban areas.

The calculated semivariograms are shown in Fig. 8, subplots (a)–(e). The area integrals were computed and compared to the mean RMSE of the June-July-August period CLARA-SAL pentad means. The JJA RMSE was chosen as a reference metric since the analyzed Landsat images of the sites were taken between late May and early August. The results of the comparison are illustrated in subplot (f) of Fig. 8. Although there are only five sites in the analysis, the results clearly suggest a correlation between heterogeneity of near-infrared surface reflectances and CLARA-SAL RMSE over a similar period. To investigate whether the varying lag distance would bias the area integrals, we also calculated area integrals over the shortest analyzed lag range of 372 Landsat pixels. The results are shown in subplot (f) of Fig. 8 in blue circles. The correlation is less strong, but still considerable.

The semivariograms show features that also correlate plausibly to actual terrain onsite. For example, the clear increase in the semivariogram estimator at Payerne when lag distance is close to 300 Landsat pixels is most likely due to the influence of Lac de Neuchâtel, a large lake northwest of Payerne. At Barrow, the coastal location of the site and the presence of several smaller water bodies nearby have been known to cause challenges for coarse-resolution imagers during surface parameter retrieval (Niu and Pinker, 2011).

5 Comparison of the dataset with MCD43C3 products

In-situ validation yields valuable information about retrieval quality at individual sites, but offers little opportunity to evaluate the product at larger scales. To accomplish this,

ACPD
12, 25573–25615, 2012

we compared CLARA-SAL to the MODIS MCD43C3 surface albedo product over the year 2009. The MODIS albedo product and its validation efforts have been extensively described in the literature (e.g. Schaaf et al., 2002; Jin et al., 2003; Cescatti et al., 2012). To match the CLARA-SAL products to the MODIS 16-day albedo means, the following procedures were followed:

- The MCD43C3 product was coarsened to 0.25° resolution by averaging 5 × 5 pixel regions with the assumption that the spatial matching is thus sufficiently good to allow a general comparison of the products.
- The MCD43C3 products are 16-day means whereas CLARA-SAL products are pentads and monthly means. For simplicity, it was decided to create a MODIS-equivalent CLARA-SAL product by averaging the pentads which fit within the MODIS 16-day period, plus minus one day. Three pentads were generally available for averaging per MODIS product.
- Areas where either CLARA-SAL or MODIS had no data-values were excluded.

The comparison results are shown in Fig. 9. The overall annual albedo cycle of both products is remarkably similar, although CLARA-SAL is consistently 10–20 % higher. The largest differences occur over areas with high cloudiness and aerosol loading, which are also probable causes for the difference. A notable and surprising exception is Sahara, where both products agree within 10 % despite the differences in AOD handling between the products.

6 Product stability and retrieval uncertainty considerations

Evaluation of the long-term stability of the CLARA-SAL timeseries requires study of a target with minimal natural variability to separate algorithm-related changes from actual natural albedo changes. We decided to use the central part of the Greenland Ice Sheet for this purpose, since its albedo is known to be stable (Stroeve et al., 1997). To

ACPD
12, 25573–25615, 2012

minimize sporadic cloud misclassfication errors, a 0.5 × 0.5° study area was selected (74.75–75.25° N, 42.25–42.75° W). We calculated the regional mean albedo from each monthly mean product between 1982–2009 and also analyzed the regional means of the number of observations-datafield and the standard deviation of the monthly mean albedo. The calculated timeseries is shown in Fig. 10.

The interannual mean albedo over central GrIS is 0.844, which is very well in line with the commonly cited albedo of dry fresh snow over GrIS (≈0.84) (Konzelmann and Ohmura, 1995). The maximum deviation from the interannual mean is 6.8 %. If our assumption that the GrIS interior has a constant albedo, this deviation may be attributed solely to CLARA-SAL retrieval uncertainty. How good is that assumption? We have included only the highest regions of central GrIS to avoid any regions that experience surface melt (Fettweis et al., 2011). On the other hand, other authors have reported some seasonal variation in the in situ surface albedo at Summit camp, in the middle of our study area (Stroeve et al., 2005). We also note that seasonal variation in Solar Zenith Angles will cause some variation in the monthly mean CLARA-SAL albedo, as the data is unnormalized in this first edition.

Riihelä et al. (2010) have discussed error sources of the operational SAL product over snow and ice, which mostly apply to this study as well. Cloud mask misclassifications cause the largest retrieval errors, but they occur only sporadically. Uncorrected atmospheric effects vary as a function of both region and time period. The retrieval error caused by ozone variation is only a few percent (relative). AOD variation effects are generally acceptable (under 5 %), but over regions with high AOD loading (see Fig. 11) the resulting retrieval error can be more than 15 %.

The algorithm also has inherent uncertainty. The narrow-to-broadband conversion algorithms have reported uncertainties of 5–10 % (Liang, 2000; Xiong et al., 2002). The BRDF correction and spectral albedo calculation for vegetation (Roujean et al., 1992; Wu et al., 1995) is estimated to have an uncertainty in the same order of magnitude.

ACPD
12, 25573–25615, 2012

7 Discussion

Our study of the first edition of the CLARA-SAL dataset has provided us with information concerning its strengths and weaknesses. While the overall albedo retrieval capability is comparable to previous AVHRR-based datasets, we are aware of certain issues which require improvement in future editions. Firstly, the accuracy of the atmospheric correction needs to be improved over high-aerosol regions. AOD datasets covering 1982 onwards are scarce, the ones used for the ERA-40 and ERA-Interim reanalysis datasets being the most analyzed (Tanré et al., 1984; Tegen et al., 1997). However, as the use of aerosol climatologies as satellite retrieval input tends to cause unwanted internal correlation between them, we are also examining methods to perform the atmospheric correction based solely on satellite data.

For AOD we use a constant of 0.1 for this first edition for two main reasons; Firstly, we could not find an appropriate global and robust aerosol dataset covering 1982–2009. Also, a sensitivity study showed that given typical vegetation reflectances and viewing/illumination geometry, the albedo retrieval error caused by using AOD of 0.1 would be only −0.8 % (relative) if actual AOD was 0.2, and −5.2 % if actual AOD was 0.3. Figure 11 shows the annual mean AOD at 555 nm for the year 2010 from the MISR instrument (Martonchik et al., 1998), highlighting regions where annual mean AOD exceeds 0.25. Sahara, the Middle East and Southeast Asia are the regions where we may expect substantial retrieval errors to occur as a result of the constant AOD in CLARA-SAL, elsewhere the error is acceptable. It should be noted that the constant AOD does create larger retrieval errors in the visible surface reflectances than stated here. However, over vegetated surfaces the near-infrared surface reflectance dominates the broadband albedo and acts to lessen the influence of AOD variation, since solar radiation at near-infrared wavelengths is scattered considerably less effectively by aerosols. Over the snow-covered polar regions the aerosol effect could be considerably larger, but in situ measured aerosol concentrations at 500 nm have typically been between 0.05 and 0.2 (Tomasi et al., 2007), ameliorating this issue.

ACPD
12, 25573–25615, 2012

Another issue which needs to be mentioned is the evolution of land cover. As the CLARA-SAL BRDF correction uses local land cover as an input variable, natural and man-made changes in both sub- and superpixel land cover can effect retrieval quality in a systematic way. In this first edition, we utilized a single Land Use Cover (LUC) dataset (USGS classfication of 1992–1993) as the basis for calculations. Updates to LUC datasets occur infrequently, but it is possible that, e.g. high temporal resolution datasets of vegetation phenology could be used to update land cover data for albedo calculations along the lines of Stöckli et al. (2011).

We are also planning improvements to the snow/ice and ocean albedo calculations. Utilization of long-term sea ice concentration datasets will remove cloud masking errors. In this first edition of the dataset, cloud masking errors over sea ice usually occur at the edges of persistent cloud fronts and/or regions with high SZA. Users are strongly recommended to utilize the number of observations-datafield to establish an appropriate screening of data for their application. We are also investigating the inclusion of a ocean wind speed dataset to improve ocean albedo representativeness.

8 Conclusions

We have developed, processed and validated a timeseries describing the global black-sky broadband surface albedo between 1982–2009. In this paper we have described the processing algorithm and validation strategy, highlighted representative validation results and discussed the stability of the dataset, as well as its comparability to the well-known MODIS black-sky albedo product. The main results of our work are as follows:

1. Validation results from 11 sites show the mean achieved retrieval accuracy to be 10–15 % relative to ground truth. Larger discrepancies are found at some sites, but an analysis of the representativeness of the in situ albedo measurements suggests that large errors result from heterogeneous land cover around the validation site.

ACPD
12, 25573–25615, 2012

2. Analysis of the interannual stability of the CLARA-SAL dataset over the inner part of the Greenland Ice Sheet shows that monthly means over the region are stable within 7 % (relative) during the 28 yr of coverage. It should be kept in mind that variations in snow precipitation and illumination geometry may cause some natural seasonal albedo variability. Interannual mean CLARA-SAL albedo over the inner part of GrIS agrees very well with the theoretical albedo of fresh dry snow as well as in situ observations.

3. Comparison of CLARA-SAL with MCD43C3 during 2009 shows similar overall features in both products, although CLARA-SAL is typically 10–20 % higher. On the same note, the retrieval accuracy for snow albedo in the CLARA-SAL dataset is comparable to the AVHRR Polar Pathfinder timeseries (Stroeve et al., 2001).

Future work on the CLARA-SAL timeseries will focus on improving the atmospheric correction and sea ice extent determination. We will also explore possibilities to enhance the land cover dataset to include natural and man-made changes, and include wind speed data into the ocean albedo calculation. Future editions of the CLARA-SAL dataset will also extend the coverage period of the dataset.

Appendix A

SAL algorithm description

CLARA-SAL processing is illustrated as a flowchart in Fig. 12. Before CLARA-SAL processing, the TOA radiances are converted to TOA reflectances considering Sun-Earth distance and local Sun Zenith Angle across each image swath. The preprocessing by the PPS module (Dybbroe et al., 2005) also creates a cloud mask and provides CLARA-SAL with Sun/satellite geometry data and a land cover classification for each pixel in the image swath. AVHRR GAC reflectances from channels 1 and 2 are used in CLARA-SAL albedo retrieval. We omit numerical details in this description.

ACPD
12, 25573–25615, 2012

First, any cloud-contaminated pixels are excluded from processing, as well as any pixels for which the Sun Zenith Angle (SZA) is larger than 70° or the Viewing Zenith Angle (VZA) is larger than 60°. The snow/ice flags in the cloud mask are used to identify snow cover and sea ice.

The topography affects the satellite image in first order in two ways: (1) the altitude difference with respect to sealevel will cause the geolocation of the pixel to be shifted and (2) the inclination of the slopes of the terrain within a pixel will alter its reflectance value. As the BRDF calculations are based on a horizontal plane assumption, erroneous values will be obtained for inclined slopes. In addition, the slope distribution of the terrain covered by the pixel may contain slopes that are not seen at all by the sun or the satellite.

The topography correction for geolocation considers the fact that latitude/longitude coordinates of a satellite pixel on the ground are calculated in AVHRR preprocessing assuming a flat Earth at sea level; at the swath edges where satellite viewing angle is large, actual location of a satellite pixel may differ considerably if the terrain is elevated. Where elevation is sufficiently high in the swath, the elevated pixel reflectance is moved onto its neighbor in the range direction, in fact replacing the original pixel. The GTOPO30 Digital Elevation Model (DEM) is used to determine pixel elevation.

The topography correction for radiometry considers the fact that AVHRR surface reflectances over sloped terrain are affected by the distribution and orientation of terrain slopes in the subpixel scale. Some slopes are not visible to the satellite, others are not illuminated by the Sun, and some are neither. Yet, they would still contribute the the overall albedo of that area, therefore their presence has to be corrected for. First, DEM slope information is utilized to determine the viewing/illumination geometry for each (subpixel) slope in the AVHRR pixel. BRDF calculations are repeated for each slope (as viewing/illumination geometry changes for each), assuming reflectance signature shapes to be identical for all slopes in the pixel. The calculated slope reflectances are averaged, and the average is adjusted to include the non-visible slopes' effect.

ACPD
12, 25573–25615, 2012

This average sloped terrain reflectance is finally compared to the observed AVHRR reflectance to obtain the correction factor.

The next processing step is to remove the atmospheric scattering and absorption effects from the imaged reflectances, transforming them from TOA reflectances into surface reflectances. We utilize the Simplified Method for Atmospheric Correction (SMAC) after Rahman and Dedieu (1994) to do this. The SMAC algorithm is a version of the Second Simulation of a Satellite Signal in the Solar Spectrum (6S) Radiative Transfer (RT) code, where some parts of the RT calculations have been parameterized to speed up the algorithm. The calculation is made separately for both AVHRR channels using continental coefficients.

The atmospheric correction requires four inputs: (1) aerosol optical depth (AOD) at 550 nm, (2) total ozone content of the atmosphere ($\mathrm{atm\,cm^{-1}}$), (3) total column water vapour ($\mathrm{g\,cm^{-2}}$), and (4) surface pressure (hPa). Surface pressure and total column water vapour are taken from the daily ERA-Interim reanalysis dataset. Ozone content of the atmosphere has typically a very small effect on visible and near-infrared radiances, therefore we use a constant value of $0.35\,\mathrm{atm\,cm^{-1}}$. After the atmospheric correction, the processing separates according to surface type. For non-snow covered land surfaces, we correct for anisotropy in the surface reflectance prior to the conversion into spectral albedo. The process uses the kernel-based BRDF/albedo model by Roujean et al. (1992), using land cover-specific BRDF coefficients from Wu et al. (1995). The derived spectral land surface albedos are finally converted into a single broadband surface albedo using the linear regression equations of Liang (2000).

For water, we employ the LookUp-Table (LUT) approach of Jin et al. (2004). In this first edition of CLARA-SAL, the water albedo is very simplistic: The four inputs of the LUT are set to constants; SZA to 60°, wind speed at surface is set to $10\,\mathrm{m\,s^{-1}}$, AOD is kept at the processing constant of 0.1, and chlorophyll content of the water surface layer is set to $0.15\,\mathrm{mg\,m^{-3}}$. Therefore ocean albedo is a constant 0.067 throughout the dataset.

ACPD
12, 25573–25615, 2012

For snow and sea ice, we keep the approach described and validated by Riihelä et al. (2010). The spectral surface reflectances are converted into broadband bidirectional reflectances using the empirical equations of Xiong et al. (2002). The conversion algorithm also accounts for ponding effects, which are important for late summer sea ice albedo retrievals. Instead of attempting an instantaneous reflection anisotropy correction, the broadband reflectances are averaged over the product period per grid cell, sampling the snow BRDF to create a snow broadband albedo estimate. Sufficient sampling of the viewing hemisphere is required to make the estimate accurate. Fortunately AVHRR overpasses occur frequently over the high-latitude regions with significant snow cover. Figure 13 illustrates a typical distribution of surface reflectance retrievals in the Viewing Zenith/Viewing Azimuth angle space at Summit Camp (72.58° N, −38.5° E) during the observable part of year 2007. Between April and August the viewing hemisphere is well sampled (between 110 and 291 retrievals per month) at this site, despite cloud cover and the viewing angle cut-off. Similar distributions have been observed at all of our high-latitude validation sites.

Acknowledgements. The authors would like to acknowledge and thank the support of the entire CM SAF project team in generation of the dataset. SHEBA data provided by NCAR/EOL under sponsorship of the National Science Foundation. The authors thank Timo Vihma and Timo Palo for the provision of Tara data. This study has been supported by the CM SAF project of EUMETSAT.

References

Cescatti, A., Marcolla, B., Santhana Vannan, S. K., Pan, J. Y., Román, M. O., Yang, X., Ciais, P., Cook, R. B., Law, B. E., Matteucci, G., Migliavacca, M., Moors, E., Richardson, A. D., Seufert, G., and Schaaf, C. B.: Intercomparison of MODIS albedo retrievals and in situ measurements across the global FLUXNET network, Remote Sens. Environ., 121, 323–334, 2012. 25588

ACPD
12, 25573–25615, 2012

Dybbroe, A., Thoss, A., and Karlsson, K.-G.: SAFNWC AVHRR cloud detection and analysis using dynamic thresholds and radiative transfer modelling Part I: Algorithm description, J. Appl. Meteorol., 44, 39–54, 2005. 25592

Fettweis, X., Tedesco, M., van den Broeke, M., and Ettema, J.: Melting trends over the Greenland ice sheet (1958–2009) from spaceborne microwave data and regional climate models, The Cryosphere, 5, 359–375, doi:10.5194/tc-5-359-2011, 2011. 25589

Gascard, J.-C., Bruemmer, B., Offermann, M., Doble, M., Wadhams, P., Forsberg, R., Hanson, S., Skourup, H., Gerland, S., Nicolaus, M., Metaxian, J.-P., Grangeon, J., Haapala, J., Rinne, E., Haas, C., Heygster, G., Jakobson, E., Palo, T., Wilkinson, J., Kaleschke, L., Claffey, K., Elder, B., and Bottenheim, J.: Exploring arctic transpolar drift during dramatic sea ice retreat, EOS T. Am. Geophys. Un., 89, 21–28, 2008. 25585

Govaerts, Y., Lattanzio, A., Taberner, M., and Pinty, B.: Generating global surface albedo products from multiple geostationary satellites, Remote Sens. Environ., 112, 2804–2816, http://www.sciencedirect.com/science/article/pii/S0034425708000412, 2008. 25577

Grenfell, T. C. and Perovich, D. K.: Spectral albedos of sea ice and incident solar irradiance in the Southern Beaufort Sea, J. Geophys. Res., 89, 3573–3580, 1984. 25585

Heidinger, A. K., Straka III, W. C., Molling, C. C., Sullivan, J. T., and Wu, X.: Deriving an inter-sensor consistent calibration for the AVHRR solar reflectance data record, Int. J. Remote Sens., 31, 6493–6517, doi:10.1080/01431161.2010.496472, 2010. 25578

Intrieri, J. M., Shupe, M. D., Uttal, T., and McCarty, B. J.: An annual cycle of Arctic cloud characteristics observed by radar and lidar at SHEBA, J. Geophys. Res., 107, 8030, doi:10.1029/2000JC000423, 2002. 25585

Jin, Y., Schaaf, C. B., Woodcock, C. E., Gao, F., Li, X., Strahler, A. H., Lucht, W., and Liang, S.: Consistency of MODIS surface bidirectional reflectance distribution function and albedo retrievals: 2. validation, J. Geophys. Res., 108, 4159, doi:10.1029/2002JD002804, 2003. 25588

Jin, Z., Charlock, T. P., Smith Jr., W. L., and Rutledge, K.: A parameterization of ocean surface albedo, Geophys. Res. Lett., 31, 22301, 2004. 25579, 25594

Karlsson, K.-G., Riihelä, A., Müller, R., Meirink, J., Sedlar, J., Stengel, M., Lockhoff, M., Trentmann, J., and Wolters, E.: CLARA GAC – The CMSAF cloud and radiation dataset from 28 years of global AVHRR data, Atmos. Chem. Phys., in preparation, 2012. 25575, 25578, 25580

ACPD
12, 25573–25615, 2012

Key, J. R., Wang, X., Stoeve, J. C., and Fowler, C.: Estimating the cloudy-sky albedo of sea ice and snow from space, J. Geophys. Res., 106, 12489–12497, 2001. 25585
Konzelmann, T. and Ohmura, A.: Radiative fluxes and their impact on the energy balance of the Greenland Ice Sheet, J. Glaciol., 41, 490–502, 1995. 25589
Liang, S.: Narrowband to broadband conversions of land surface albedo I: Algorithms, Remote Sens. Environ., 76, 213–238, 2000. 25579, 25582, 25589, 25594
Liu, J., Schaaf, C., Strahler, A., Jiao, Z., Shuai, Y., Zhang, Q., Roman, M., Augustine, J. A., and Dutton, E. G.: Validation of Moderate Resolution Imaging Spectroradiometer (MODIS) albedo retrieval algorithm: dependence of albedo on solar zenith angle, J. Geophys. Res., 114, D01106, doi:10.1029/2008JD009969, 2009. 25580
Loew, A. and Govaerts, Y.: Towards Multidecadal Consistent Meteosat Surface Albedo Time Series, Remote Sens., 2, 957–967, doi:10.3390/rs2040957, http://www.mdpi.com/2072-4292/2/4/957/, 2010. 25577
Lucht, W., Hymana, A. H., Strahler, A. H., Barnsley, M. J., Hobson, P., and Muller, J.-P.: A Comparison of satellite-derived spectral albedos to ground-based broadband albedo measurements modeled to satellite spatial scale for a semidesert landscape, Remote Sens. Environ., 74, 85–98, 2000. 25576, 25582
Manninen, T., Riihelä, A., and de Leeuw, G.: Atmospheric effect on the ground-based measurements of broadband surface albedo, Atmos. Meas. Tech. Discuss., 5, 385–409, doi:10.5194/amtd-5-385-2012, 2012. 25580
Martonchik, J., Diner, D. J., Kahn, R., Ackerman, T. P., Verstraete, M. M., Pinty, B., and Gordon, H. R.: Techniques for the retrieval of aerosol properties over land and ocean using multi-angle imaging, IEEE T. Geosci. Remote, 36, 1212–1227, 1998. 25590
Matheron, G.: Principles of geostatistics, Econ. Geol., 58, 1246–1266, 1963. 25581
Niu, X. and Pinker, R. T.: Radiative fluxes at barrow, Alaska: a satellite view, J. Climate, 24, 5494–5505, 2011. 25587
Ohmura, A., Gilgen, H., Hegner, H., Müller, G., Wild, M., Dutton, E. G., Forgan, B., Fröhlich, C., Philipona, R., Heimo, A., König-Langlo, G., McArthur, B., Pinker, R., Whitlock, C. H., and Dehne, K.: Baseline Surface Radiation Network (BSRN/WCRP): new precision radiometry for climate research., B. Am. Meteorol. Soc., 79, 2115–2136, doi:10.1175/1520-0477(1998)079<2115:BSRNBW>2.0.CO;2, 1998. 25579
Perovich, D., Grenfell, T., Light, B., and Hobbs, P.: Seasonal evolution of the albedo of multiyear Arctic sea ice, J. Geophys. Res., 107, 1–13, 2002. 25585

ACPD
12, 25573–25615, 2012

Rahman, H. and Dedieu, G.: SMAC: a simplified method for the atmospheric correction of satellite measurements in the solar spectrum, Int. J. Remote Sens., 15, 123–143, 1994. 25578, 25594

Riihelä, A., Laine, V., Manninen, T., Palo, T., and Vihma, T.: Validation of the Climate-SAF surface broadband albedo product: comparisons with in situ observations over Greenland and the ice-covered Arctic Ocean, Remote Sens. Environ., 114, 2779–2790, 2010. 25584, 25586, 25589, 25595

Román, M. O., Schaaf, C. B., Woodcock, C. E., Strahler, A. H., Yang, X., Braswell, R. H., Curtis, P. S., Davis, K. J., Dragoni, D., Goulden, M. L., Gu, L., Hollinger, D. Y., Kolb, T. E., Meyers, T. P., Munger, J. W., Privette, J. L., Richardson, A. D., Wilson, T. B., and Wofsy, S. C.: The MODIS (Collection V005) BRDF/albedo product: Assessment of spatial representativeness over forested landscapes, Remote Sens. Environ., 113, 2476–2498, 2009. 25581, 25582

Rossow, W. B. and Schiffer, R. A.: Advances in understanding clouds from ISCCP, B. Am. Meteorol. Soc., 80, 2261–2287, 1999. 25577

Roujean, J.-L., Leroy, M., and Deschamps, P.-Y.: A bidirectional reflectance model of the Earth's surface for the correction of remote sensing data, J. Geophys. Res., 97, 20455–20468, 1992. 25579, 25589, 25594

Rutan, D., Rose, F., Roman, M., Manalo-Smith, N., Schaaf, C., and Charlock, T.: Development and assessment of broadband surface albedo from clouds and the Earth's radiant energy system clouds and radiation swath data product, J. Geophys. Res., 114, D08125, doi:10.1029/2008JD010669, 2009. 25577

Schaaf, C. B., Gao, F., Strahler, A. H., Lucht, W., Li, X., Tsang, T., Strugnell, N. C., Zhang, X., Jin, Y., Muller, J.-P., Lewis, P., Barnsley, M., Hobson, P., Disney, M., Roberts, G., Dunderdale, M., Doll, C., d´Entremont, R. P., Hu, B., Liang, S., Privette, J. L., and Roy, D.: First operational BRDF, albedo nadir reflectance products from MODIS, Remote Sens. Environ., 83, 135–148, 2002. 25588

Schaepman-Strub, G., Schaepman, M. E., Painter, T. H., Dangel, S., and Martonchik, J. V.: Reflectance quantities in optical remote sensing definitions and case studies, Remote Sens. Environ., 103, 27–42, 2006. 25576

Stackhouse, P. W., Gupta, S. K., Cox, S. J., Zhang, T., Mikovitz, J., and Hinkelman, L. M.: 24.5-yr SRB Data Set Released, in: GEWEX News, vol. 21, WCRP, Silver Spring, USA, 2011. 25577

ACPD

12, 25573–25615, 2012

Steffen, K., Box, J., and Abdalati, W.: Greenland Climate Network: GC-Net, CRREL 96-27 Special Report on Glaciers, Ice Sheets and Volcanoes, tribute to Meier, M., 98–103, 1996. 25579

Stöckli, R., Rutishauser, T., Baker, I., Liniger, M. A., and Denning, A. S.: A global reanalysis of vegetation phenology, J. Geophys. Res., 116, G03020, doi:10.1029/2010JG001545, 2011. 25591

Stroeve, J., Nolin, A., and Steffen, K.: Comparison of AVHRR – derived and in situ surface albedo over the Greenland ice sheet, Remote Sens. Environ., 62, 262–276, 1997. 25584, 25588

Stroeve, J. C., Box, J. E., Fowler, C., Haran, T., and Key, J.: Intercomparison between in situ and AVHRR polar pathfinder-derived surface Albedo over Greenland, Remote Sens. Environ., 75, 360–374, 2001. 25580, 25592

Stroeve, J. C., Box, J. E., Gao, F., Liang, S., Nolin, A., and Schaaf, C.: Accuracy assessment of the MODIS 16-day albedo product for snow: comparisons with Greenland in situ measurements, Remote Sens. Environ., 94, 46–60, 2005. 25584, 25589

Stroeve, J. C., Box, J. E., and Haran, T.: Evaluation of the MODIS (MOD10A1) daily snow product over the Greenland ice sheet, Remote Sens. Environ., 105, 155–171, 2006. 25584

Susaki, J., Yasuoka, Y., Kajiwara, K., Honda, Y., and Hara, K.: Validation of MODIS Albedo Products of Paddy Fields in Japan, Geoscience and Remote Sensing, IEEE Transactions on, 45, 206–217, 2007. 25581

Tanré, D., Geleyn, J.-F., and Slingo, J.: First results of the introduction of an advanced aerosol-radiation interaction in the ECMWF low resolution global model, in: Aerosols and their Climatic Effects, edited by: Gerber, H. and Deepak, A., A. Deepak publishing: Hampton, VA, USA, 133–177, 1984. 25590

Tegen, I., Hollrig, P., Chin, M., Fung, I., Jacob, D., and Penner, J.: Contribution of different aerosol species to the global aerosol extinction optical thickness: estimates from model results, J. Geophys. Res., 102, 23895–23915, doi:10.1029/97JD01864, 1997. 25590

Tomasi, C., Vitale, V., Lupi, A., Di Carmine, C., Campanelli, M., Herber, A., Treffeisen, R., Stone, R. S., Andrews, E., Sharma, S., Radionov, V., von Hoyningen-Huene, W., Stebel, K., Hansen, G. H., Myhre, C. L., Wehrli, C., Aaltonen, V., Lihavainen, H., Virkkula, A., Hillamo, R., Ström, J., Toledano, C., Cachorro, V. E., Ortiz, P., de Frutos, A. M., Blindheim, S., Frioud, M., Gausa, M., Zielinski, T., Petelski, T., and Yamanouchi, T.: Aerosols in polar regions: a his-

ACPD
12, 25573–25615, 2012

torical overview based on optical depth and in situ observations, J. Geophys. Res., 112, D16205, doi:10.1029/2007JD008432, 2007. 25590

Trenberth, K., Moore, B., Karl, T., and Nobre, C.: Monitoring and prediction of the earth's climate: a future perspective, J. Climate (CLIVAR special issue), 19, 5001–5008, doi:10.1175/JCLI3897.1, 2006. 25575

Wang, X. and Key, J. R.: Arctic surface, cloud, and radiation properties based on the AVHRR polar pathfinder dataset. Part I: Spatial and temporal characteristics, J. Climate, 18, 2558–2574, 2005. 25576

Wu, A., Li, Z., and Cihlar, J.: Effects of land cover type and greenness on advanced very high resolution radiometer bidirectional reflectances: analysis and removal, J. Geophys. Res., 100, 9179–9192, 1995. 25579, 25589, 25594

Xiong, X., Stamnes, K., and Lubin, D.: Surface albedo over the arctic ocean derived from AVHRR and its validation with SHEBA data, J. Appl. Meteorol., 41, 413–425, 2002. 25579, 25589, 25595

Zhang, Y., Rossow, W. B., Lacis, A. A., Oinas, V., and Mishchenko, M. I.: Calculation of radiative fluxes from the surface to top of atmosphere based on ISCCP and other global data sets: refinements of the radiative transfer model and the input data, J. Geophys. Res., 109, D19105, doi:10.1029/2003JD004457, 2004. 25577

ACPD

12, 25573–25615, 2012

Table 1. The validation sites used in this study.

Site	Latitude North (deg)	Longitude East (deg)	Validation period
Barrow, USA	71.32	−156.61	1995–2009
Neumayer, Antarctica	−70.65	−8.25	1995–2009
Payerne, Switzerland	46.82	6.95	1995–2009
Southern Great Plains, USA	36.61	−97.49	1994–2009
Syowa, Antarctica	−69.00	39.59	1998–2009
Tateno, Japan	36.05	140.13	1997–2009
Sodankylä, Finland	67.37	26.63	1999–2009
DYE-2, Greenland	66.48	−46.28	1996–2009
JAR-2, Greenland	69.42	−50.06	1999–2007, 2009
Summit camp, Greenland	72.58	−38.50	1995–2005, 2007–2009
SHEBA ice camp	variable	variable	1998
Tara ice camp	variable	variable	2007

ACPD
12, 25573–25615, 2012

Table 2. Validation results over the full validation period at each site.

Site	Pentad mean RMSE	Monthly mean RMSE	mean relative retrieval error of 3-month periods (%)			
			DJF	MAM	JJA	SON
Barrow	0.144	0.102	–	−10.75	−12.01	−39.74
Neumayer	0.174	0.173	−13.52	−17.92	–	−8.56
Payerne	0.110	0.110	−42.79	−46.65	−41.61	−42.46
SGP	0.043	0.038	−11.06	−9.37	−10.23	−12.29
Syowa	0.175	0.188	−2.85	−2.68	–	−13.88
Tateno	0.078	0.070	−38.96	−22.90	+6.46	−22.64
Sodankylä	0.089	0.087	–	−19.64	+3.26	+12.92
DYE-2	0.041	0.036	–	+1.40	+2.17	−0.71
JAR-2	0.082	0.064	–	+5.34	+7.68	+6.01
Summit camp	0.062	0.042	–	+4.37	+2.54	−0.20
SHEBA ice camp	0.081	–	–	–	–	–
Tara ice camp	0.090	–	–	–	–	–

ACPD
12, 25573–25615, 2012

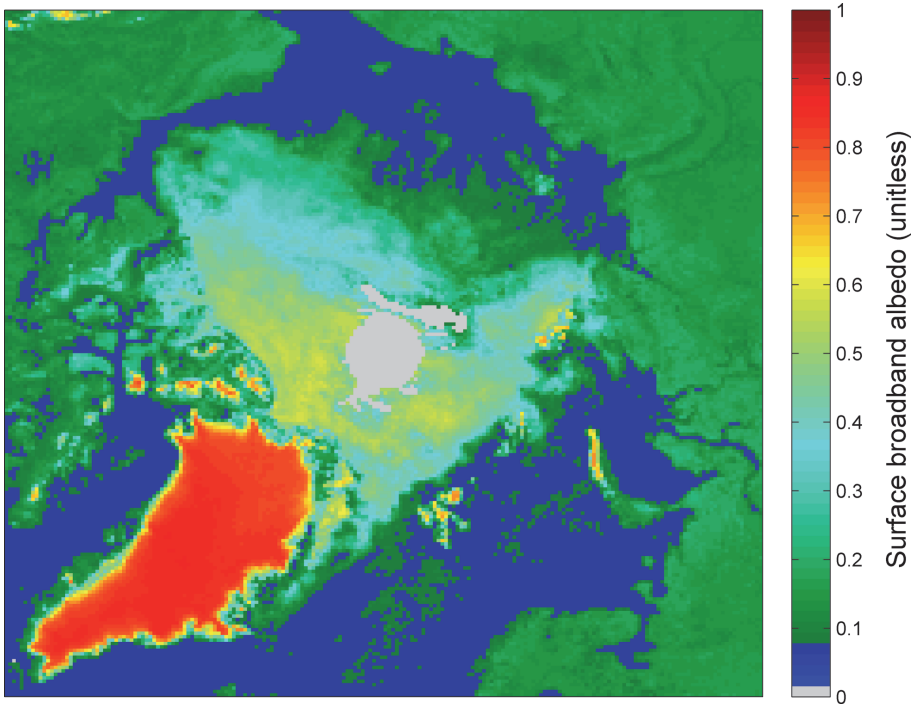

Fig. 1. An example of the Arctic CLARA-SAL monthly mean product from August 2007. Grid cell size is 25 km.

ACPD
12, 25573–25615, 2012

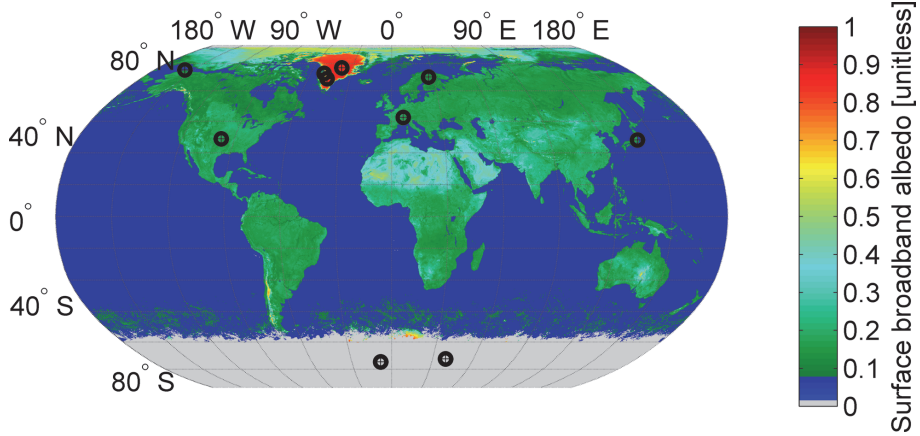

Fig. 2. An example of the global lat-long grid CLARA-SAL monthly mean product from August 2007. The grid cell resolution is 0.25°. Validation sites are overlaid using black cross-in-circle markers.

ACPD
12, 25573–25615, 2012

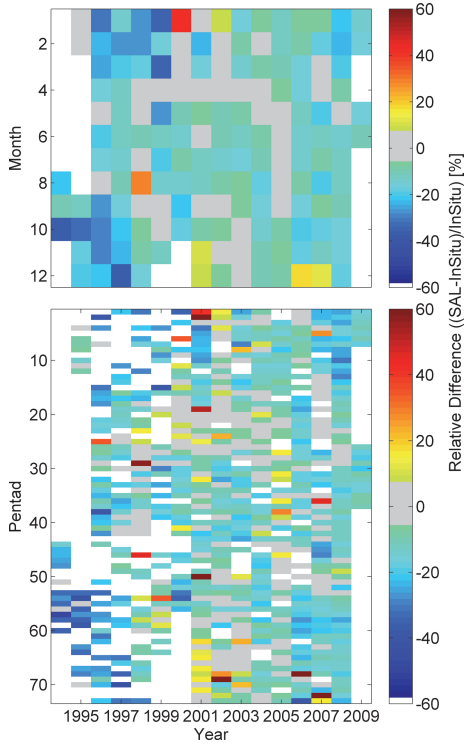

Fig. 3. The relative retrieval error of CLARA-SAL at SGP between 1994–2009. Upper subplot indicates color-coded relative retrievals errors of monthly means, the lower subplot shows the same for pentad means. The grey color indicates a retrieval error within ±5 %. Cells with white color indicate non-available satellite or in situ data.

ACPD
12, 25573–25615, 2012

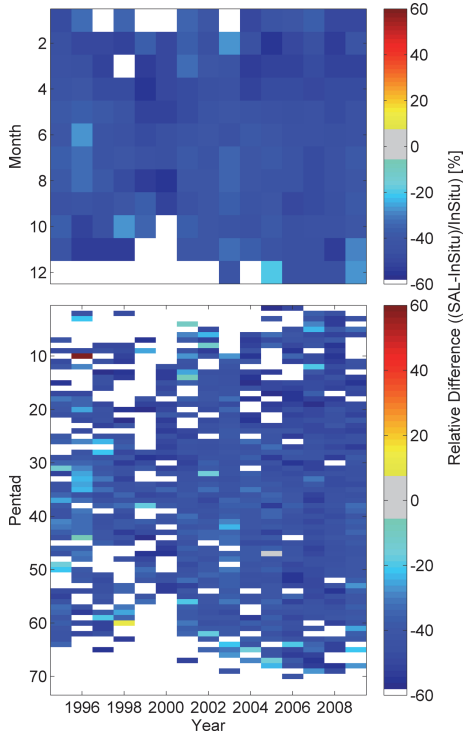

Fig. 4. As Fig. 3, but at Payerne between 1995–2009.

ACPD
12, 25573–25615, 2012

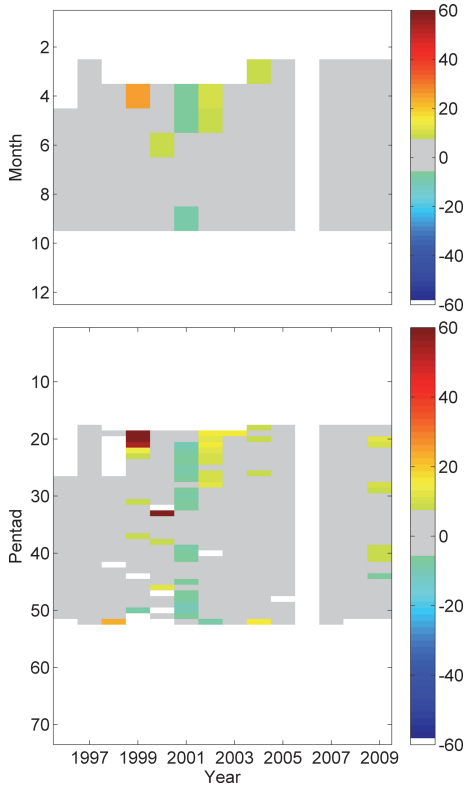

Fig. 5. As Fig. 3, but at Summit camp between 1996–2005 and 2007–2009.

ACPD
12, 25573–25615, 2012

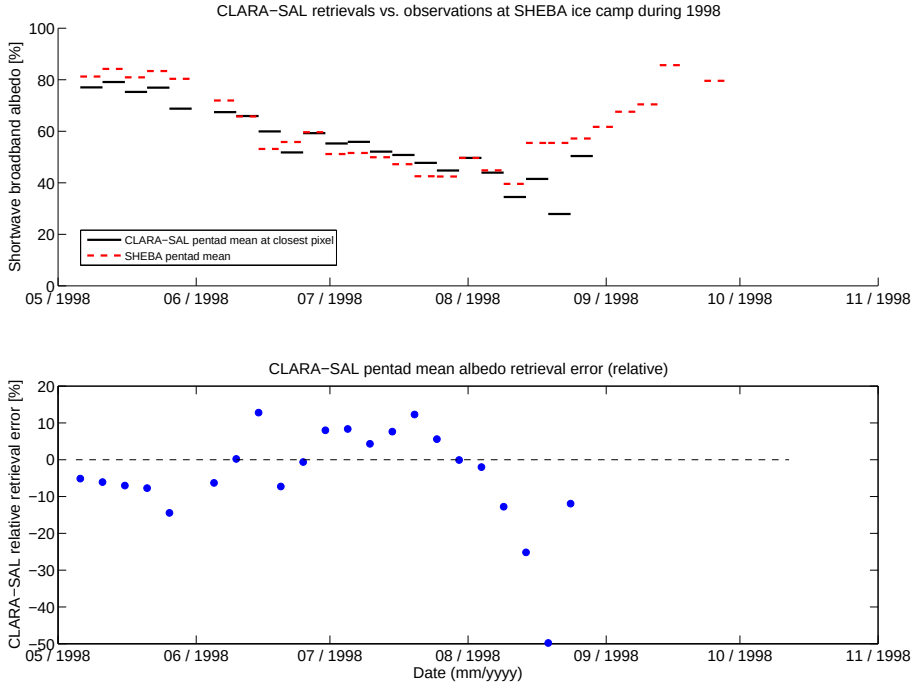

Fig. 6. Validation results of CLARA-SAL pentad means against corresponding in situ pentad albedo means at the SHEBA ice camp during 1998. Upper figure: Retrieved albedos. Lower figure: Relative retrieval accuracy of CLARA-SAL against in situ data.

ACPD
12, 25573–25615, 2012

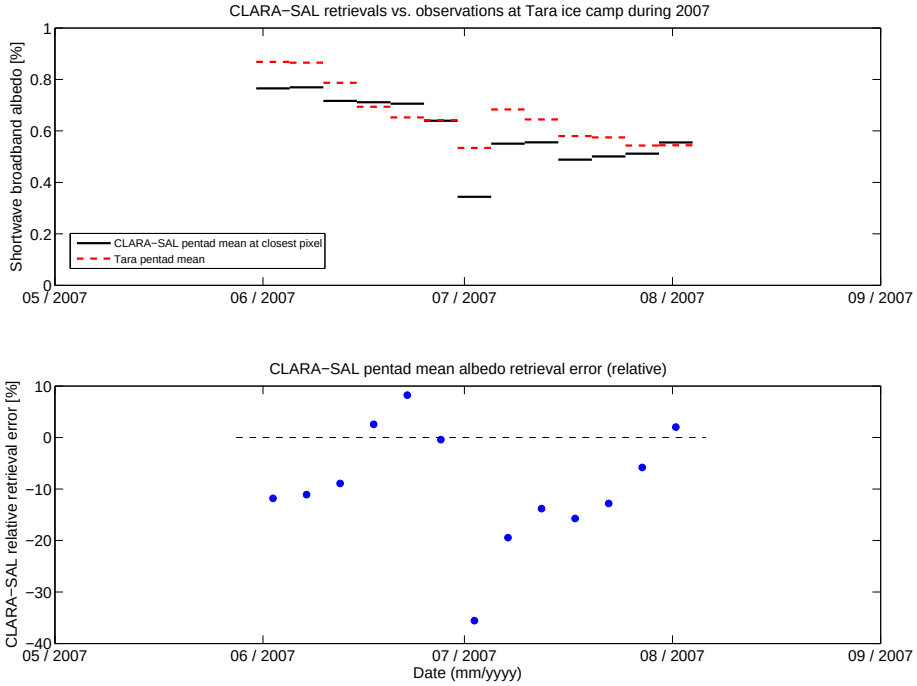

Fig. 7. As Fig. 6, but for Tara ice camp data from 2007.

ACPD
12, 25573–25615, 2012

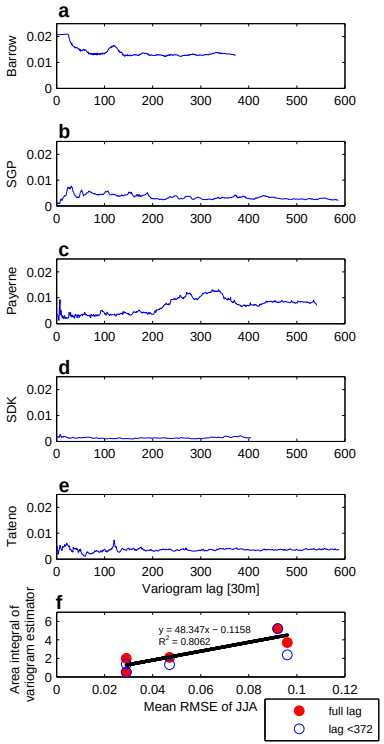

Fig. 8. Variogram estimators of Landsat channel 4 surface reflectance for **(a)** Barrow, **(b)** Southern Great Plains, **(c)** Payerne, **(d)** Sodankylä, **(e)** Tateno. Subplot **(f)** shows the correlation between the mean RMSE error of CLARA-SAL during the summer months and the area integral of the variogram estimator for full lag length in a CLARA-SAL 0.25° pixel (red circles), and the area integral corresponding to the shortest full lag length in the set (blue circles). The linear fit shown in **(f)** is for the full lag length correlation.

ACPD
12, 25573–25615, 2012

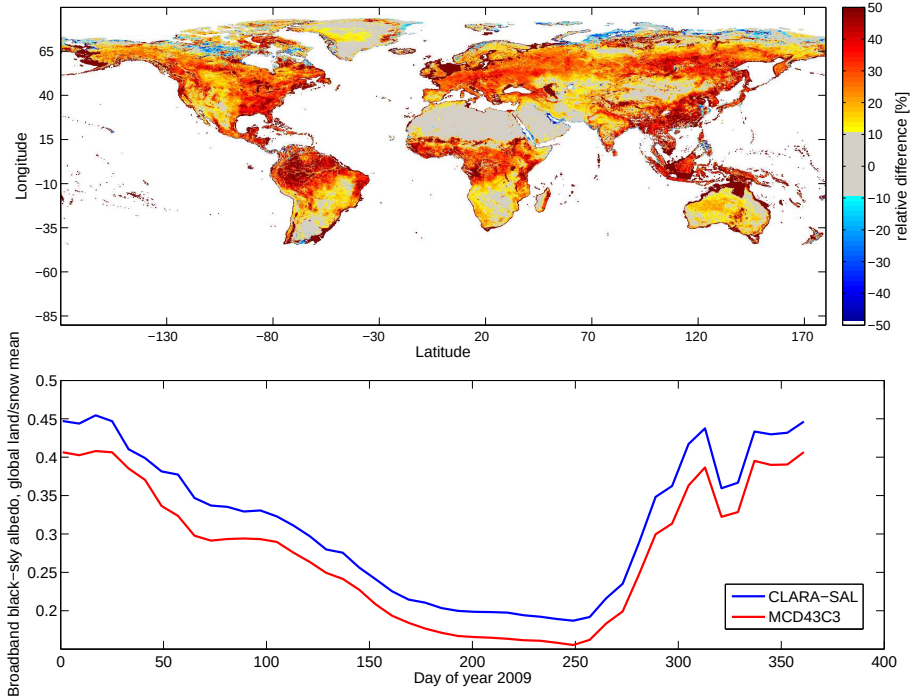

Fig. 9. Upper subplot: Relative difference between CLARA-SAL and MCD43C3 during the 16-day period starting on day of year 145. Land and snow surfaces considered. Grey color indicates difference of less than ±10 %. Lower subplot: CLARA-SAL and MCD43C3 mean retrievable black-sky albedo over land/snow surfaces through 2009. Relative difference varies generally between 10 and 20 %.

ACPD
12, 25573–25615, 2012

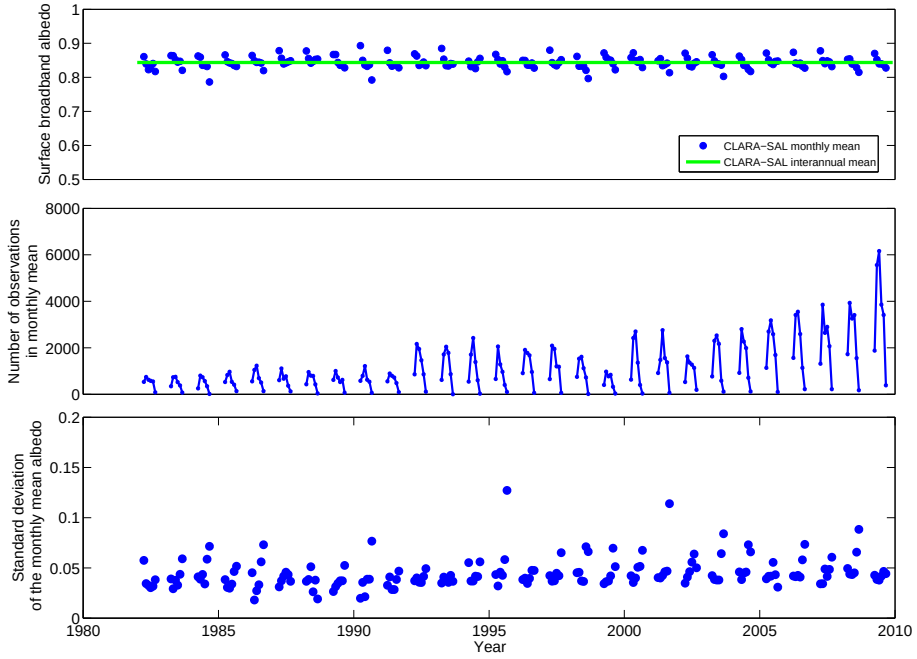

Fig. 10. Subplot **(a)** illustrates the monthly means of surface albedo over 28 yr, averaged over the central part of GrIS. The thick green line shows the 28 yr mean albedo of the region. Subplot **(b)** shows the mean number of AVHRR overpasses in each monthly mean in **(a)**, averaged over the study region. Finally, subplot **(c)** shows the mean standard deviation of each monthly mean in **(a)**, averaged over the study region.

ACPD
12, 25573–25615, 2012

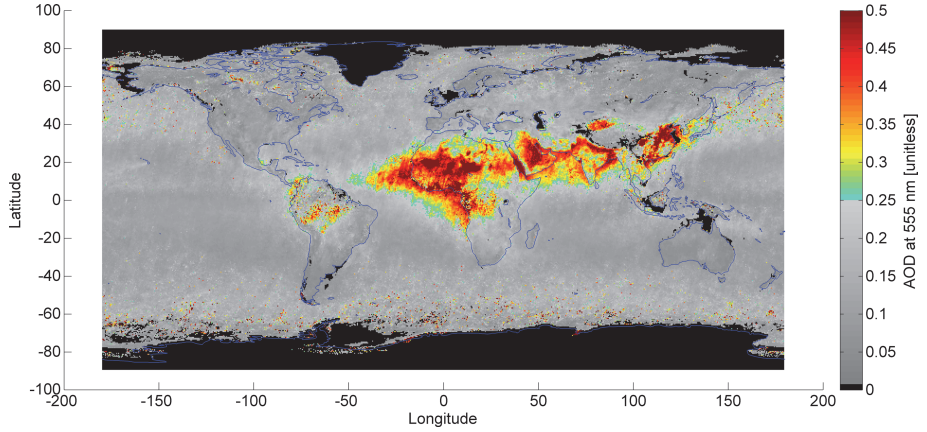

Fig. 11. The global annual mean AOD at 555 nm from the MISR AOD product for the year 2010. Color coding set to highlight regions where the annual mean exceeds 0.25; full range of data not shown.

ACPD
12, 25573–25615, 2012

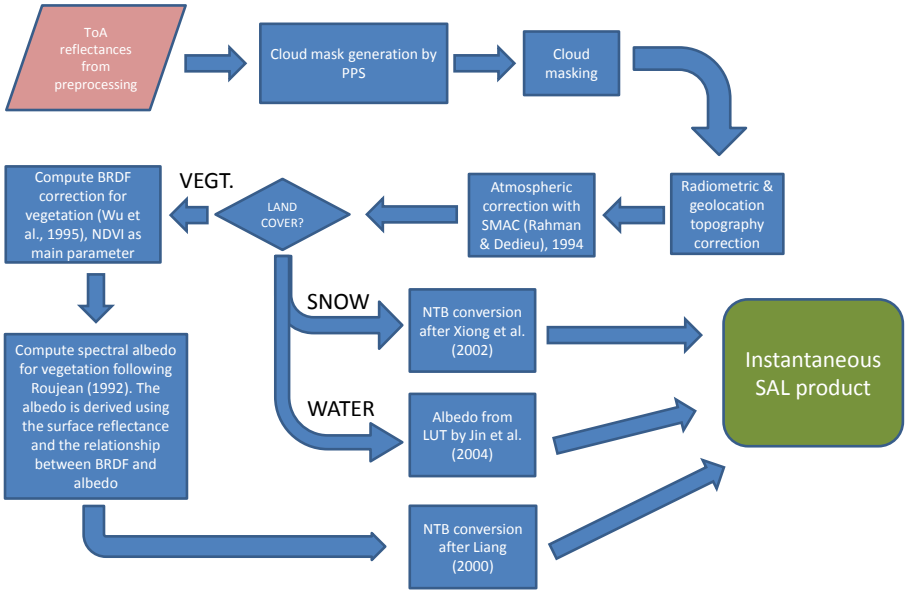

Fig. 12. The SAL algorihm process as a flowchart.

ACPD
12, 25573–25615, 2012

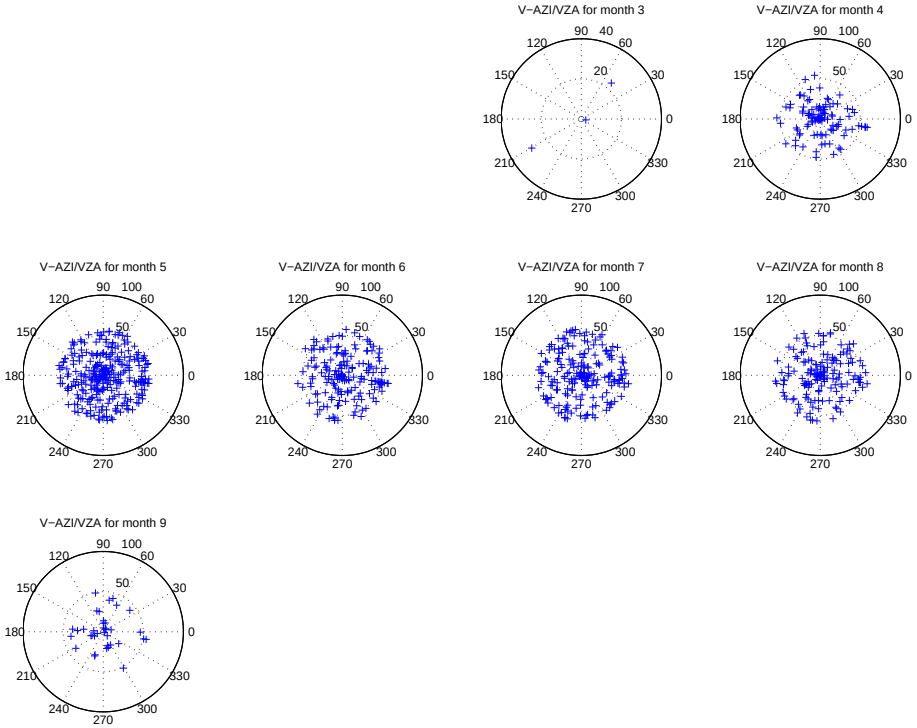

Fig. 13. Sampling of the viewing hemisphere in AVHRR surface reflectance retrievals at Summit Camp on the Greenland Ice Sheet during 2007. Radial direction indicates increasing Viewing Zenith Angle, the azimuth direction indicates increasing Viewing Azimuth Angle.

ACPD
12, 25573–25615, 2012